Title	A combined experimental–numerical investigation of fracture of polycrystalline cubic boron nitride
Authors(s)	Carolan, Declan, Ivankovic, Alojz, Murphy, Neal
Publication date	2013-02
Publication information	Carolan, Declan, Alojz Ivankovic, and Neal Murphy. "A Combined Experimental–numerical Investigation of Fracture of Polycrystalline Cubic Boron Nitride" 99 (February, 2013).
Publisher	Elsevier
Item record/more information	http://hdl.handle.net/10197/4599
Publisher's statement	This is the author's version of a work that was accepted for publication in Engineering Fracture Mechanics. Changes resulting from the publishing process, such as peer review, editing, corrections, structural formatting, and other quality control mechanisms may not be reflected in this document. Changes may have been made to this work since it was submitted for publication. A definitive version was subsequently published in Engineering Fracture Mechanics (99, , (2013)) DOI: http://dx.doi/org/10.1016/j.engfracmech.2012.09.008
Publisher's version (DOI)	10.1016/j.engfracmech.2012.09.008

A Combined Experimental-Numerical Investigation of Fracture of Polycrystalline Cubic Boron Nitride

D. Carolan[a,*], A. Ivanković[a], N. Murphy[a]

[a]*School of Mechanical and Materials Engineering, University College Dublin, Ireland*

Abstract

Numerical modelling of a series of experimental Single Edge V-Notched Beam tests was carried out for a number of grades of polycrystalline cubic boron nitride using the finite volume method (FV) and cohesive zone model approach. The effect of notch root radius observed experimentally was reproduced numerically via a unique CZM for each material examined. It was also found that the shape of the cohesive zone model can be significant, especially when the material has a relatively high fracture energy. It was also demonstrated that the experimentally observed drop in fracture toughness with increase in test rate was not explainable in terms of the system dynamics. It was found that in order to predict the experimental fracture loads for a range of loading rates, it was necessary to modify the CZM in such a way as to preserve the micro-structural length scale information of the material embedded within the CZM.

Keywords: brittle fracture, cohesive zone model, finite volume method, OpenFOAM-ext

---

*Corresponding Author
Email address: `declan.carolan@ucd.ie` (D. Carolan)

1. Introduction

Over the last 25 years, Polycrystalline Cubic Boron Nitride (PCBN) has become an increasingly important tool choice for the efficient machining of hard ferrous materials. This is, in part, due to a desire to reduce cost while increasing tool performance. Customers, in particular, the aerospace [1, 2] and automotive industries [3, 4, 5, 6] require a cutting tool that will give a long tool life and deliver precision and consistency to the machining operation over the life of the tool. In addition, parts are now being machined out of aerospace or other abrasive alloys which would present major challenges with conventional tooling. An ideal cutting material should possess the following material characteristics:

- Extremely high hardness.

- Good toughness.

- High thermal conductivity.

- Chemical inertness.

Typical property values for the main categories of cutting tool materials are shown in Figure 1 [7]. Polycrystalline Diamond (PCD) outperforms all the other tool materials in almost all cases, with the notable exception of fracture toughness. However, PCD is not suitable for use in ferrous metalworking since it is chemically unstable in the presence of iron [8]. The diamond particles in a PCD compact begin to decompose into graphite at 700°C. This is a major limitation for the use of PCD, as around 80% of common workpiece materials are ferrous [9]. PCBN, on the other hand is thermally stable and
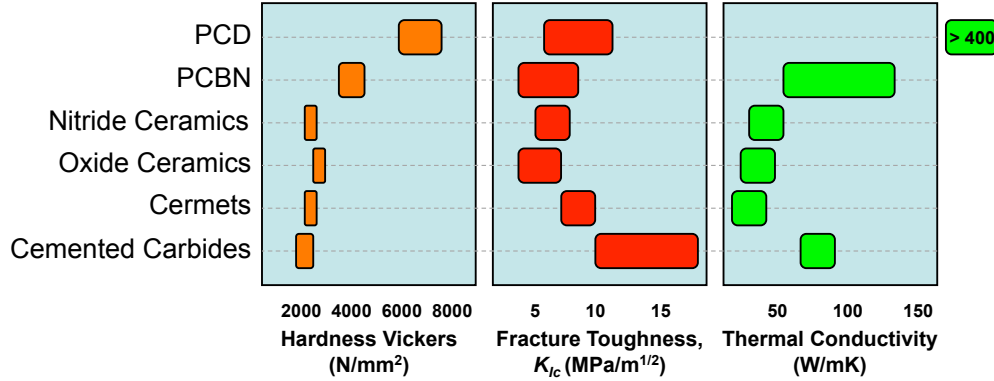
Figure 1: Typical values for the properties for the main classes of cutting tool materials. After [7].

highly resistant to chemical attack. As a result, the high temperatures which occur near the tip of the cutting tool do not pose difficulties and can be used to promote hot cutting when machining ferrous metals, making it an excellent choice of tool material for the metalworking industry. The heat induced soft cutting means that the PCBN tool is not in contact with the workpiece in its hardened state which greatly improves the tool life when compared with other cutting tool materials [10]. PCBN tooling is also effective in the machining of softer, but highly abrasive grey cast irons.

The superior characteristics of PCBN make it ideally suited to both high speed and dry machining where the adoption of advanced cutting practices, such as minimum quantity lubricant (MQL) and ultra high speed machining, substantially increase the economic viability of using the more expensive PCBN tooling [10].

3

Cubic Boron Nitride (CBN), a synthetic material, is the second hardest material in the world. PCBN, as used for cutting tools, is a sintered mass of CBN particles of the order of 1-25 μm with a variety of ceramic and metal phases. The end product is a bulk material with a unique combination of high hot hardness and chemical stability which are increasingly important in the metal cutting industry today. However failure due to fracture and chipping is still a major problem in the industry. In order to improve the fracture toughness of these materials it is firstly necessary to fully characterize the fracture properties and the underlying fracture mechanisms of the material under a wide range of operating conditions. This requires undertaking fundamental research into the properties of the material and the behaviour of PCBN in the cutting process.

The effect of a characteristic length scale on the experimentally measured fracture toughness of materials has been investigated analytically by a number of researchers, notably by Taylor [11, 12, 13], Carolan et al. [14] and Elices et al. [15]. These authors have shown that the characteristic length scale can be related back to the microstructure of the material. The current work shows that the characteristic length scale or microstructural information is embedded within the cohesive zone formulation and affects the fracture behaviour of the material under a range of loading conditions.

2. Experimental Method

In this work fracture tests were performed on PCBN Single Edge V-Notched Beam (SEVNB) specimens. The fracture toughness of two grades of PCBN, denoted A and B, was evaluated at a number of crosshead dis-

4

placement rates from 1 mm/min to 1 m/s, and at a number of different temperatures between room temperature and 750°C. The fracture toughness of a further three grades, denoted C, D and E, was determined at 1 mm/min and room temperature.

2.1. Low Rate Tests

Low rate tests were performed using a screw driven tensile testing machine, type Hounsfield H50KS. Three different crosshead displacement rates were applied, 1 mm/min, 10 mm/min and 350 mm/min. In addition to this five different test temperatures were prescribed, up to 750°C. The load was measured using a 10 kN load cell. The fracture toughness, K_{Ic}, was evaluated using the load at initiation method [16]. The main assumption of this analysis is that linear elastic fracture mechanics (LEFM) can provide a realistic description of the stress field at initiation. A schematic and photo of the test setup used can be seen in Figure 2. Fracture toughness was then evaluated using Equation (1).

$$K_{Ic} = \frac{P_{in}s}{bh^{3/2}} \cdot f(\alpha) \tag{1}$$

where s is the span , P_{in} is the breaking load, $\alpha = a/h$, where a is initial crack length and f is a calibration function given by Equation (2).

$$f(\alpha) = \frac{3\alpha^{0.5}[1.99 - \alpha(1 - \alpha)(2.15 - 3.93\alpha + 2.7\alpha^2)]}{2(1 + 2\alpha)(1 - \alpha^2)^{1.5}} \tag{2}$$

2.2. High Rate Tests

As outlined in Section 2.1 the accuracy of the load at fracture analysis depends on a precise determination of the crack initiation load. Determination of this load at high rates can be rather more complicated due to inertia
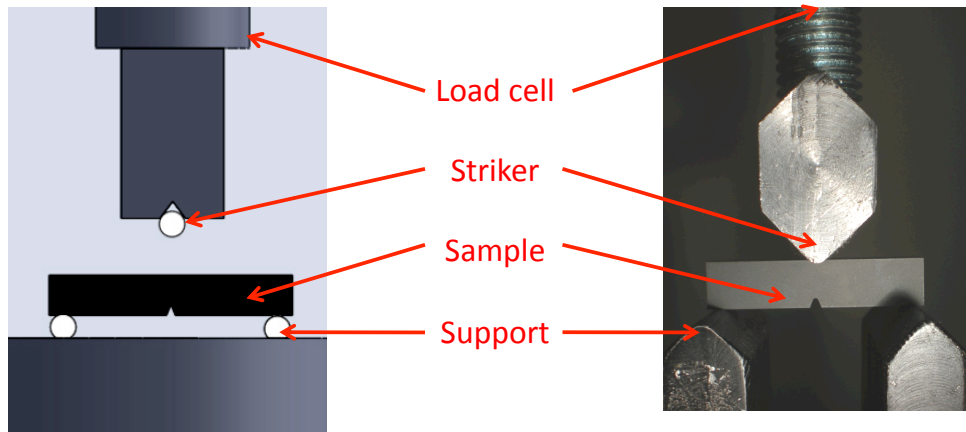
Figure 2: Low rate TPB test.

and stress wave propagation effects. Hence, at the initiation of fracture, the fracture load does not necessarily have to coincide with the peak load on the load time trace obtained by the machine load cell.

According to Belenky et al. [17], there are three main categories for measuring dynamic fracture toughness: high rate bending, high rate tension and dynamic wedging. The majority of investigations have attempted to extend existing quasi-static techniques to a dynamic loading situation, hence the proliferation of high rate bending techniques. The bend test can be one-, three- or four-point with the load provided by a modified Hopkinson bar, a drop tower, a high rate servo-hydraulic machine or a Charpy pendulum [18]. Both Belenky et al. [17] and Kim and Chao [19] reported significant increases in fracture toughness at increased loading rates for monolithic ceramics.

Kalthoff at al. [20] showed that the dynamic effects at the crack tip were significantly smaller than the load measured at the striker contact point. It follows then, that there exists a unique relationship between the dynamic

fracture toughness of the material and the time to fracture initiation. Weis-brod and Rittel [21] have also used the time to initiation method to measure the dynamic fracture toughness using a one point bend impact configuration. They measured the time for fracture initiation via a small strain gauge placed close to the crack tip and measuring the strain at this point as a function of time during the fracture event. This strain gauge can also be can be used as a load cell if calibrated beforehand under static conditions. The precalibrated strain gauge approach is used in the current work to determine the fracture load.

In the current work a minute strain gauge (type: Vishay EA-015LA-120, gauge length: 0.38 mm), designated as the tip strain gauge (TSG) was bonded close to the crack tip for all high rate tests to record the fracture initiation time, t_f and fracture initiation strain ϵ_f. A photo of a fractured specimen with the strain gauge still attached close to the crack tip is given in Figure 3.

Initial testing incorporated a small trigger circuit attached to the top of the sample as shown in Figure 4. The intention of this trigger circuit was to facilitate precise determination of the point at which the striker contacts the specimen. However it was subsequently found that given the small size of the sample and the proximity of the TSG to the trigger line that the closing of the trigger circuit resulted in a substantial voltage spike in the strain gauge output. In addition to this the trigger did not fire until sufficient contact pressure was applied between the striker and the trigger line. This meant that the contact circuit could not be used as an accurate measure of the onset of loading. To simplify the experimental arrangement, a light gate was

used to trigger the recording of the TSG signal. The strain was recorded on a *Handyscope HS3* 100 MHz signal conditioning amplifier, while the load was recorded by a 25 MHz amplifier. The time at which loading of the sample began, t_s was then determined directly from the TSG signal by the intersection of two straight lines as shown in Figure 5. The time to fracture, t_f, was measured as the time difference between the initiation time and peak value of the TSG signal.
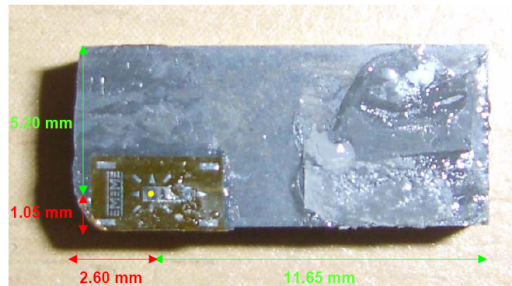

Figure 3: Fractured Specimen showing position of TSG.

3. Experimental Results

The experimentally determined fracture toughnesses for all rate temperature combinations of PCBN A and PCBN B are plotted in Figures 6 and 7 respectively. The nominal crosshead displacement rates varied from 1 mm/min (1.67×10^{-5} m/s) to 1 m/s. The test temperatures varied from room temperature, 20°C to 750°C, close to the operating temperature of the tool material. At least three repeats were performed at each rate temperature combination. The fracture toughnesses were calculated using the load at initiation method. Only low rate tests were conducted at higher temperatures. This was due to
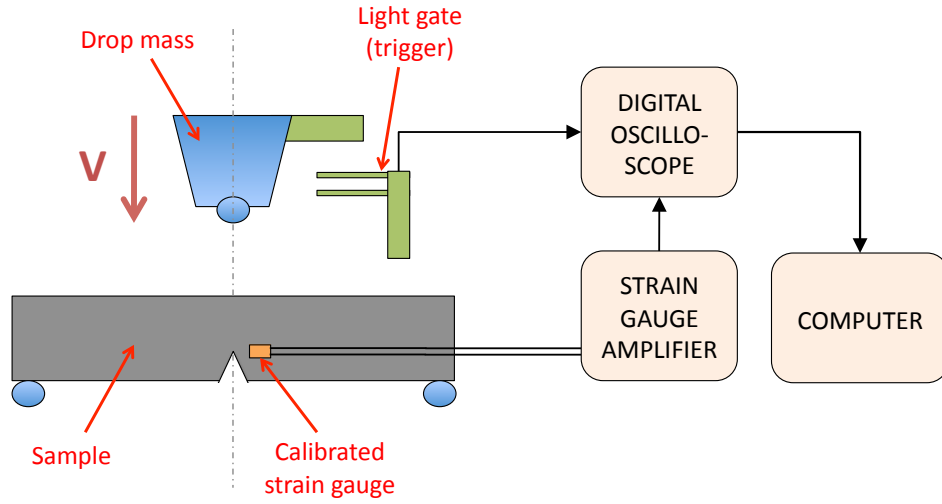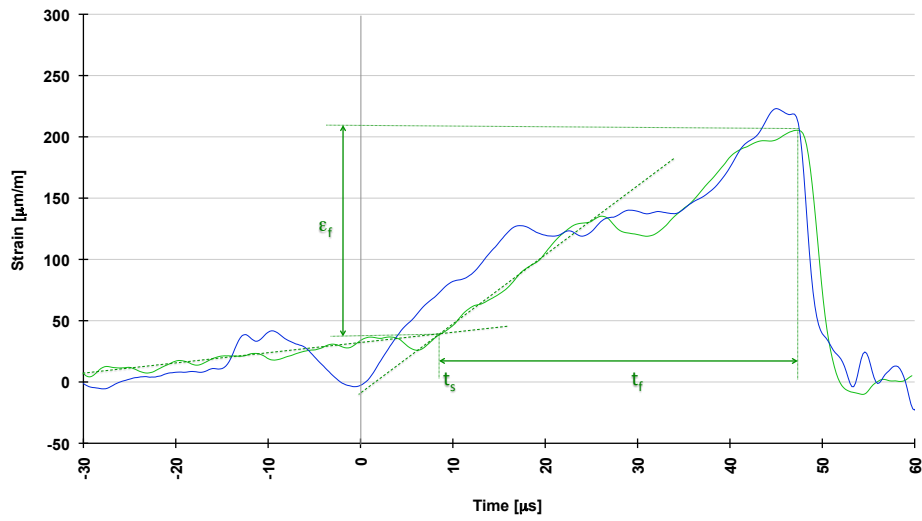
Figure 4: Schematic of the high rate TPB test.

Figure 5: Two typical strain time traces for PCBN B for a drop velocity of 0.3 m/s.

9

the expense of high temperature gauges needed to evaluate fracture toughness at high rates. Petrović [22] has successfully used these high temperature gauges to measure the dynamic fracture properties of PCD up to 650°C.
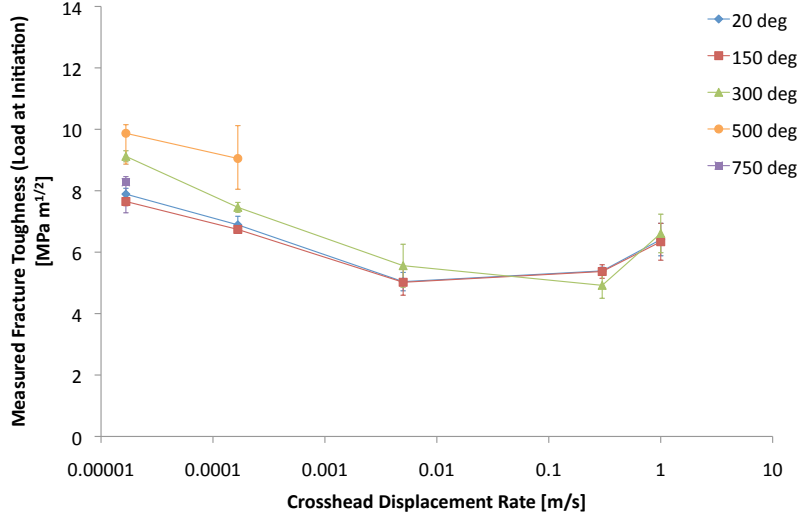

Figure 6: Variation of apparent fracture toughness with rate and temperature for PCBN A.

It should be noted that Figures 6 and 7 plot apparent or measured fracture toughnesses, denoted K_b rather than the critical fracture toughness, denoted K_c. It is known that the effect of the blunt notch plays a role in the systematic overestimation of the fracture toughness [23]. A detailed analysis of the effect of notch root radius on the measured fracture toughness for the materials used in the current work can be found in [14]. The average notch root radius for PCBN A was approximately 120 μm while for PCBN B the average notch root radius was 150 μm. The apparent fracture toughness, K_b for PCBN A, 7.7 MPa m$^{1/2}$, at low rate and low temperature was less than 7% greater than the calculated critical fracture toughness, K_{Ic} of 7.2 MPa m$^{1/2}$, whereas
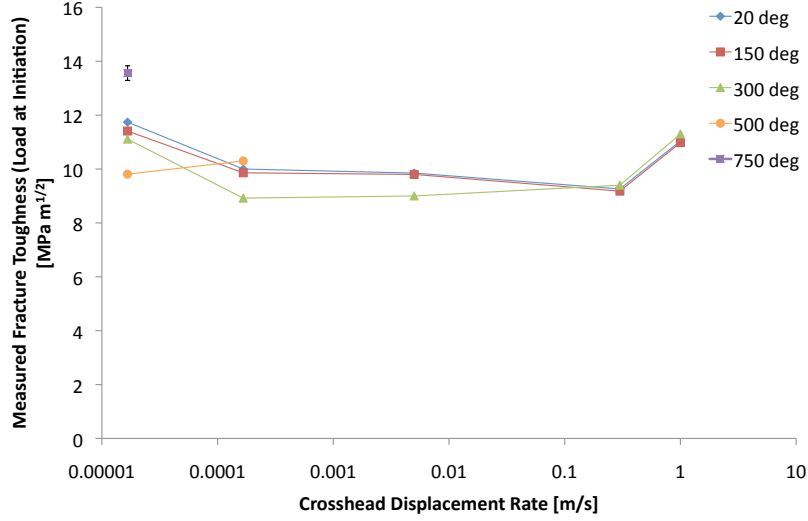
10

Figure 7: Variation of apparent fracture toughness with rate and temperature for PCBN B.

K_b for PCBN B, 11.9 MPa m$^{1/2}$, was 5.4 times greater than the measured critical fracture toughness of 2.2 MPa m$^{1/2}$.

The degree to which fracture toughness is over estimated by a blunt notched specimen over a sharp cracked specimen can be found by including a micro-structural length scale, r_c, in the maximum circumferential stress criterion proposed by Ritchie [24]:

$$K_b = K_{Ic} \frac{\left(1 + \dfrac{R}{2r_c}\right)^{\frac{3}{2}}}{1 + \dfrac{R}{r_c}} \tag{3}$$

It has been shown by Carolan *et al.* [14] that, in the case of PCBN, the microstructural length scale is always equal to the nominal CBN grain size.

A large drop in K_b was noted for PCBN A with increase in loading rate, while no significant statistical decrease was noted for PCBN B over the range

11

of test rates. Significant variation in measured fracture toughness was noted for both materials at different test temperatures. However, no consistent trend was noted with increase in test temperature. It is speculated that the measured difference in K_b values at increased test temperatures is due to the relief of the existing residual stress state caused by the manufacture of the specimen. This hypothesis was not investigated further in this work.

The critical fracture toughness, grain size, and critical distance evaluated using Equation 3 for the five grades investigated in this work are give in Table 1. It should be noted that the calculated critical distance, r_c, is very close to the nominal CBN grain size for all grades examined. In the case of PCBN A the range of notch root radii available for experimentation was not sufficient to determine a value of r_c with any degree of certainty using Equation 3. However it is shown in this work, using a cohesive zone model approach, that an r_c value equal to the given grain size of 22 μm fits the experimental data well.

Grade	K_{Ic} [MPa m$^{1/2}$]	Grain size [μm]	r_c [μm]
PCBN A	7.7	22	n/a
PCBN B	2.8	1	0.97±0.34
PCBN C	2.2	1.5	1.47±0.56
PCBN D	4.9	3	3.15±0.43
PCBN E	3.8	3	3.04±0.27

Table 1: Critical fracture toughness, grain size and critical distance of PCBN grades.

4. Finite Volume Method

The finite volume (FV) method describes a family of numerical procedures that can be used to discretise the governing equations of continuum mechanics into a system of algebraic equations. The method was first developed for the solution of solid mechanics problems by Demirdzić *et al.* [25] and Ivanković *et al.* [26]. The simplicity of the formulation has meant that the FV method is gradually gaining acceptance as an alternative to the pre-eminent finite element (FE) method for solving solid mechanics problems. It has already been used in a wide range of applications from the fracture of polymers [27, 28], adhesives [29], viscoelastic materials [30] and problems involving fluid structure interaction [31, 27]. In addition memory utilisation is very efficient. The FV method offers several major advantages including [32]:

- Relying on the laws of mass, momentum and energy conservation in their original integral form, the method is conservative, yet can be implemented relatively simply.

- It employs a segregated solution, since the equations are linearised and the set of equations for each dependent variable are decoupled. This results in very efficient memory management.

- Equations are solved sequentially using an iterative solver. This makes the method inherently suitable for the solution of non-linear problems.

- The FV method is conservative, which makes it appropriate for cohesive failure models as they are implemented along cell faces where equilibrium is considered.

4.1. OpenFOAM

All of the simulations in the current work were conducted using OpenFOAM-1.6-ext [33, 34]. OpenFOAM (Open Source Field Operation and Manipulation) software is a fully 3-dimensional, finite volume, object oriented C++ library. It is used primarily to create solvers to solve complex physics problems. One of the main strengths of OpenFOAM is that new powerful solvers and utilities can be created by a user provided the user has a solid understanding of the underlying FV methods, physics and programming techniques involved. OpenFOAM is divided into a set of pre-compiled libraries that are dynamically linked during compilation of solvers and utilities. A solver is usually designed to solve a specific computational continuum mechanics problem, while utilities perform pre- and post-processing tasks, such as meshing and data manipulation. The main theme of the design of OpenFOAM is that the solver applications being modelled have a syntax that resembles the partial differential equation being solved. This makes programming of the method relatively straightforward. For example, the equation

$$\frac{\partial(\rho V)}{\partial t} + \nabla.\phi V - \nabla.\mu\nabla V = -\nabla p \tag{4}$$

is represented by the code as:

```
solve
    (
    fvm::ddt(rho,V)
    + fvm::div(phi, V)
    - fvm::laplacian(mu, V)
    ==
```

```
    -fvc::grad(p)
    )
```

Finite volume method (`fvm`) returns a FV matrix from the discretisation of a geometric (volume) field while finite volume calculus (`fvc`) returns a geometric field. In other words `fvm` is used to treat implicit terms while `fvc` is used to treat explicit terms.

5. Modelling the TPB Test

In the present work, the simulation of pure Mode I crack growth in the TPB test is considered. The PCBN is initially treated as a homogeneous material. Only normal separation along a prescribed crack path is modelled. This is clearly a simplification of the actual fracture process which is rather more complex, involving a combination of both intergranular and transgranular fracture as well as micro-cracking adjacent to the main crack path. The tractions transmitted across the assumed crack path are related to the opening displacement of the cohesive layer via a cohesive zone (CZ) law along the interface. Before the normal tractions on the crack path cell faces reach the cohesive strength of the material, the cohesive surface behaves in the same manner as the bulk material and is modelled using the `symmetryPlane` boundary condition. Once the stress level on the cell face reaches the cohesive strength, σ_{max}, representing the onset of damage, the material behaves according to the prescribed CZM.

5.1. Mesh Generation

Figure 8 shows the typical finite volume representation of the three point bend notched specimen. A patch is a term specific to OpenFOAM which

15

encompasses one or more areas of the boundary surface which may or may not be physically connected. A number of meshes with different notch root radius geometries were created, from 1 μm to 500 μm. The boundary conditions shown in Figure 8 are also OpenFOAM specific and correspond to the following:

- `tractionDisplacement`: specifies a traction and/or displacement in x, y, z on the surface. In this case the surface is set to be traction free.

- `directionMixed`: is a mixed boundary condition which allows a combination of both a fixed value, `fixedValue`, and a fixed gradient, `fixedGradient`, boundary condition. The mixing factor is controlled in OpenFOAM by the `valueFraction` variable. Furthermore, the `directionMixed` boundary condition allows for directional decomposition into the normal and tangential directions.

- `cohesive`: is the boundary condition along which the cohesive model is implemented. The tractions on the boundary are specified according to the prescribed cohesive zone formulation.

- `symmetryPlane`: is OpenFOAM's nomenclature for a plane of symmetry.

Each mesh was created in 2-D (1 cell through thickness) and plane strain conditions were specified. The meshes were defined using `blockMesh`, OpenFOAM's built in meshing utility. The advantage of using this utility over other commercial packages is that it allows for very easy manipulation of single aspects of a complex geometry, for example, varying the notch root
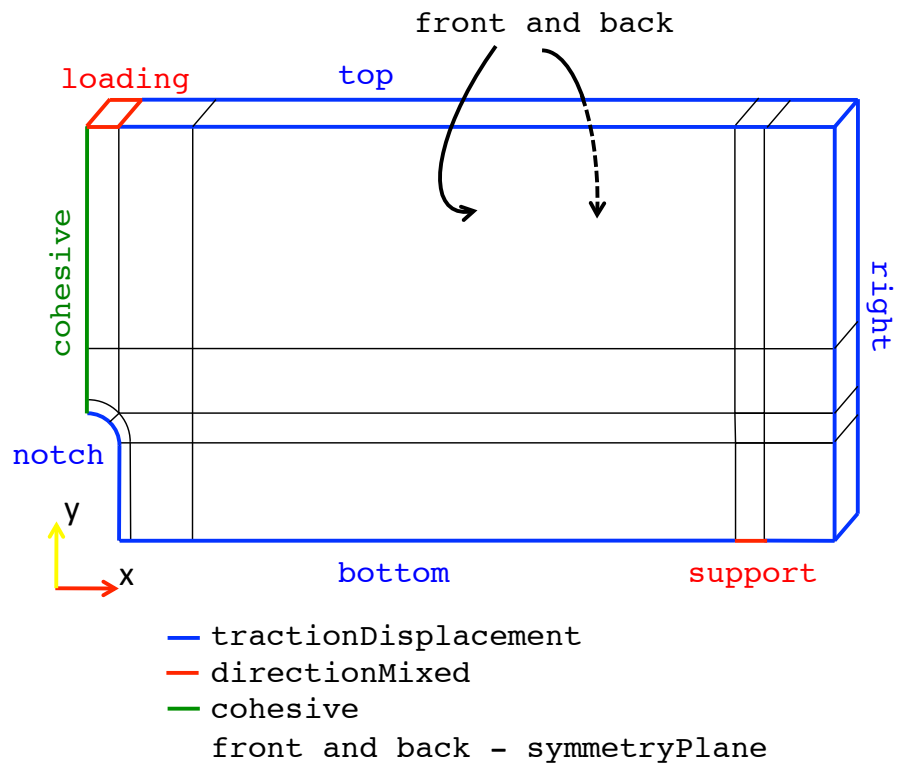
16

Figure 8: Finite volume geometry of TPB specimen with predefined crack path showing patches and OF specific boundary conditions.

radius (NRR) in a three point bend specimen. This allows for a numerical prediction of the failure load at any notch root radius and a comparison with the analytical technique described in [14] can then be made. Because of the symmetry of the problem it is only necessary to model one half of the total geometry.

5.2. Influence of Elastic Compliance of Test Rig

Numerical simulations were performed for each notch geometry for quasi-static loading, (loading rate = 1mm/min), using both a linear type and a Dugdale type cohesive law. It was found that the fracture times were considerably less, up to 50%, than those observed experimentally. An elastic support and striker as described by [35] was specified numerically in order to account for the machine loop compliance during the fracture test. A reasonable stiffness value can be obtained by considering the striker and supports as simple cylinders and then calculating the respective stiffness using $k = EA/L$ The effect of an elastic support on both the load time trace and crack growth behaviour after fracture of the sample is clearly shown in Figure 9. It should be noted that inclusion of an elastic support in the solver greatly affected the convergence characteristics of the solver for each time step. As an example, a TPB with NRR = 100 μm loaded at a crosshead displacement rate of 1 mm/min with initial time step set to 1 ms is considered. The solution for the first time step converged to a tolerance of 1×10^{-06} after 144 outer iteration in a time of 11,360 s when a rigid support was specified, whereas for an elastic support with stiffness 5 MN/m the solution had only converged to a tolerance of 0.01 after 1,000 iterations in a time of 146,537 s. Specification of an extremely compliant support (stiffness < 2 MN/m) caused the solution

18

to diverge for all time steps examined.

Inclusion of an elastic support does not affect the failure load at low rates. It does, however affect the measured striker and support loads at higher rates. However, the striker load cannot be used as a reliable measure of crack tip load as explained previously. The solver was adapted to output the strain at a predefined face close to the notch tip at the approximate location of the tip strain gauge in the instrumented test specimens. It is this measure of strain which was used to estimate the crack tip load.

For the sake of reduced computing time, it was decided to dispense with specifying the support and striker stiffness for all TPB simulations. This has the obvious effect of affecting the crack propagation phase of the simulation. However, since no experimental evidence of the crack propagation phase (such as the evolution of crack length as a function of time) was collected in the current work, propagation is not currently of interest. A complete analysis would require the incorporation of contact procedures at both the striker and supports [36].

5.3. Mesh Sensitivity

Figure 10 shows the results of a simple mesh sensitivity study on two TPB geometries with different NRR. As the main region of interest is confined to the development of the stress field around the notch tip, it is appropriate that the best measure of sensitivity be the number of cells around the notch arc rather than the total number of cells in the entire model. For both cases, there is relatively little change in predicted fracture load once there is 100 cells around the notch arc shown in Figure 8. All subsequent TPB geometries then had at least this amount of cells prescribed around the notch arc.
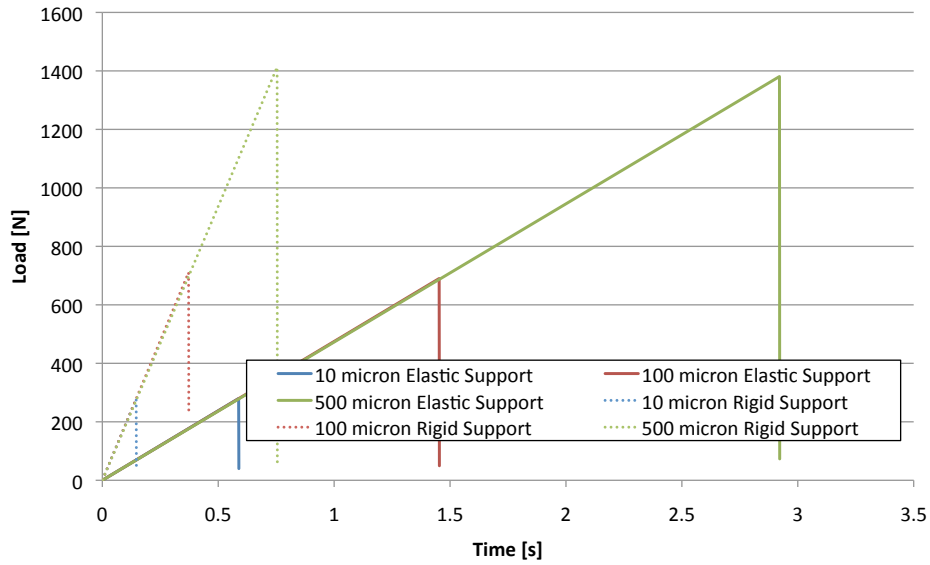
Figure 9: Numerical Load time traces for PCBN B, NRR = 10 μm, 100 μm and 500 μm. The solid lines show the numerical prediction with a elastic support ($k = 1.43$ MN/m) while the dotted lines represent the load-time traces for a completely rigid support. A linear CZM, $\sigma_{max} = 1000$ MPa, $G_{Ic} = 11$ J/m^2 was used.
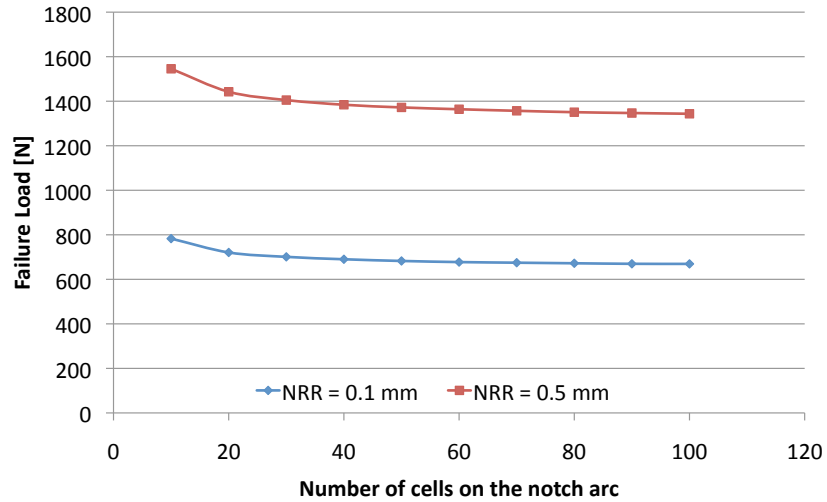

Figure 10: Effect of mesh density around the notch on numerically predicted failure for PCBN B, for two values of NRR. $G_{Ic} = 11$ J/m^2, $\sigma_{max} = 1000$ MPa, CZM type = linear.

20

5.4. CZM Parameter Sensitivity

Numerical predictions for different notch root radii may have different sensitivities to the two cohesive parameters, G_{Ic} and σ_{max}. In particular, it is important to investigate whether there is more than one set of cohesive parameters which allow a characteristic geometry to be modelled. An essential aspect of ensuring that the correct cohesive parameters are specified is a sensitivity analysis for each test geometry modelled.

5.5. Effect of CZM Shape

The effect of CZM shape has been reported to have an influence on the predicted failure of brittle materials as discussed by Chandra [37], Rots [38]. Figure 11 presents schematically the shape of four simple cohesive zone models, Dugdale, weak bilinear, linear and strong bilinear. Table 2 gives the values of $\delta_{c,i}$ used in Figures 12. Each CZM has the same fracture energy, G_{Ic}, and cohesive strength, σ_{max}. They differ only in the slope of the softening part of the cohesive curve, ranging from Dugdale, which has zero slope to what has been termed strong bilinear, which has a steep slope.

Figures 12 and 13 present the effects of the initial steepness of the cohesive zone formulation on the predicted failure load of both PCBN A and PCBN B. This effect has been presented for a sharp notch, NRR = 10 μm, and a blunt notch, NRR = 150 μm, for both materials. These notch root radii approximately represent the sharpened and unsharpened experimental test specimen geometries.

It can be seen in Figure 12 that the shape of the CZM model has no effect on the failure load for the sharp initial notch with NRR = 10 μm. This is obvious if one considers the micro-structural criteria for an equivalent sharp

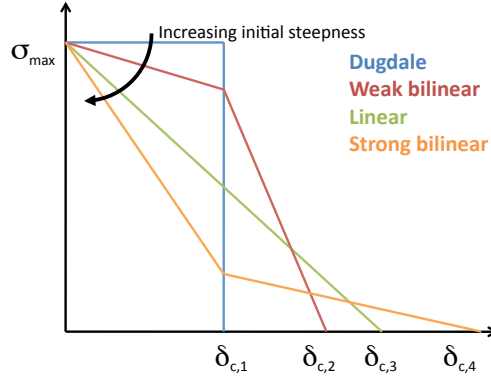Figure 11: Schematic of CZM models with increasing slope of the damage region.

Type	σ_{max} [MPa]	$\delta_{c,1}$ [μm]	$\delta_{c,2}$ [μm]	$\delta_{c,3}$ [μm]	$\delta_{c,4}$ [μm]
Dugdale	600	0.117			
Weak bilinear	600	0.117	0.155		
Linear	600			0.233	
Strong bilinear	600	0.117			8.17

Table 2: CZM parameters used in Figure 11 for PCBN A. $G_{Ic} = 70$ J/m^2 in all cases.
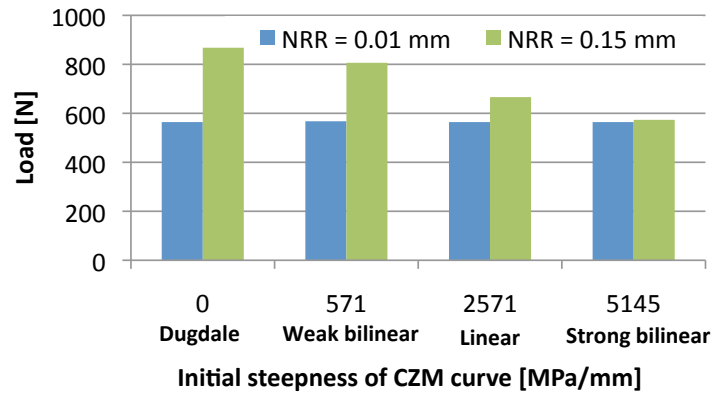
Figure 12: Effect of CZM shape on PCBN A ($G_{Ic} = 70$ J/m^2, $\sigma_{max} = 600$ MPa on a sharp notch, NRR $= 10$ μm, and a blunt notch, NRR $= 150$ μm.

22
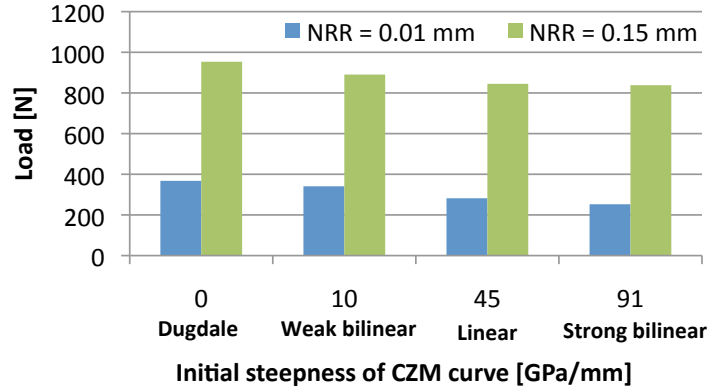
Figure 13: Effect of CZM shape on PCBN B ($G_{Ic} = 11$ J/m^2, $\sigma_{max} = 1000$ MPa on a sharp notch, NRR = 10 μm, and a blunt notch, NRR = 150 μm.

crack expressed by Damani [23] and Kübler [39] and discussed in the case of PCBN in [14]. The critical distance information is embedded within the cohesive model and the 10 μm notch root radius is much less than the value of r_c calculated for PCBN A.

A decrease in predicted fracture load was observed for the initial blunt notch. In this case the notch root radius is much more than r_c. It was found that the Dugdale model could not predict the failure load accurately for both sharp notched and blunt notched experiments. A linear model gives much more accurate predictions. This agrees with the findings of both Chandra [37] and Rots [38] who found in studies on concrete that if the damage stems from processes such as microcracking, as is the case with ceramics, rather than plasticity, as with metals, a linear or bilinear cohesive zone law is better suited to predicting damage than a Dugdale model.

PCBN B is a much less tough material than PCBN A and has a smaller critical distance, limited by the CBN grain size. Both the sharp notch and

the blunt notch exhibit a decrease in the numerically predicted fracture load with increasing initial steepness. This can be explained by the fact that both notch root radii examined are significantly in excess of the critical distance, r_c. Furthermore, the rate of decrease in both cases is approximately similar, indicating that the the choice of cohesive zone shape is not important providing that the cohesive zone parameters, G_{Ic} and σ_{max} give good agreement with the experimental results.. This is because for all the experimental geometries tested for the failure of PCBN B is very much dominated by the choice of σ_{max} and G_{Ic} plays a minor role.

6. Comparison with Experimental and Analytical Results

Table 3 lists the CZM parameters used in the current study. The fracture energy G_{Ic} was derived from experimentally determined fracture toughness. σ_{max} was found for PCBN A and PCBN B via an inverse analysis technique [40]. The measured flexural strength reported in [41] was used as an initial estimate for σ_{max}. In both cases this was found to be much too low to satisfy the experimentally determined failure loads as shown. The cohesive strength, σ_{max}, was subsequently increased until a good fit with the experimental data was obtained. The effect of both G_{Ic} and σ_{max} on the predicted failure loads of notched specimens with different notch root radii for both PCBN A and PCBN B are shown in Figures 14 - 17. Several simulations with notch root radii varying from 10 μm to 500 μ in steps of 10 μm were used to generate a curve for each cohesive zone formulation.

A comparison of Figures 16 and 17 reveal that varying σ_{max} causes the numerically predicted fracture load to diverge at large values of R/r_c, while

24

varying G_{Ic} causes the numerically predicted fracture load to diverge at low values of R/r_c. This indicates that fracture of blunt notches is mainly dominated by σ_{max}, a strength criterion, while the fracture of progressively sharper initial notches is influenced by the value of G_{Ic}. This is intuitively obvious, since only atomically sharp cracks provide an absolute measure of fracture toughness, while extremely blunt notches tend towards a measure of flexural strength. However it has been shown by Carolan et al. [14] if the notch tip radius is greater than $3.2r_c$ then the computed fracture toughness is sufficiently close to the actual fracture toughness. Indeed, most experimental measurements taken in this work are neither measures of strength nor of toughness but rather a combination of both parameters.

Grade	G_{Ic} [J/m²]	σ_{max} [MPa]	CZM type
PCBN A	70	600	Linear
PCBN B	11	1000	Dugdale
PCBN C	8.7	730	Dugdale
PCBN D	38.5	1120	Linear
PCBN E	19.9	875	Linear

Table 3: CZM parameters used in the current work.

It was noted in the preceding experimental work that the CBN grain size played a fundamental role in governing the overall fracture behaviour of PCBN specimens. Considering the fundamental critical distance relation:

$$\sigma = \frac{K}{\sqrt{2\pi r}} \tag{5}$$

and noting that at fracture, $K = K_{Ic}$, $\sigma = \sigma_{max}$ and $r = r_c$, it follows that:

$$\sigma_{max} = \frac{K_{Ic}}{\sqrt{2\pi r_c}} \tag{6}$$

Rearranging for r_c yields:

$$r_c = \left(\frac{K_{Ic}}{\sigma_{max}}\right)^2 \frac{1}{2\pi} \tag{7}$$

Inserting values obtained from numerical analysis for both PCBN A and PCBN B and noting that $G_{Ic} = K_{Ic}^2(1 - \nu^2)/E$, it is found that $r_{c,A} = 22.9$ μm and $r_{c,B} = 0.85$ μm. Both values are remarkably close to the given CBN grain sizes of 22 μm and 1 μm respectively.

The idea of a constant critical distance equal to the CBN grain size was subsequently applied to the numerical analysis of PCBN C, PCBN D and PCBN E. In each case, the critical distance, r_c was assumed to be constant and equal to the given grain size and K_{Ic} was taken from experimental analysis. σ_{max} was then calculated via Equation (6). The numerical predictions of failure load are shown in Figures 18 - 20. Very good agreement is observed between the experimental data and the numerical predictions, although it should be noted in the case of PCBN C, PCBN D and PCBN E the numerical predictions tend to underestimate the failure load. In some cases a linear CZM model was employed while in other case a Dugdale model was employed. This is detailed in a parametric study on CZM shape in Section 5.5. In general, a linear CZM is specified for the tougher materials while the shape is less important for PCBN materials with low values of G.
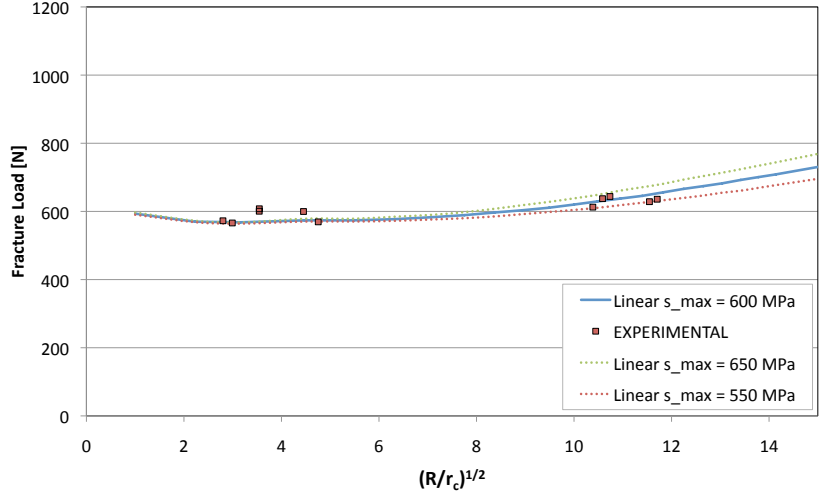
Figure 14: The effect of varying σ_{max} on the fracture load of PCBN A for a variety of normalised notch root radii, R/r_c. G_{Ic} was fixed as 70 J/m^2 for all cases and r_c was assumed to be 22 μm. The crosshead displacement rate was 1 mm/min. Results are for linear CZM.

7. Dynamic Effects

Figure 21 (a) plots the numerically predicted striker load and notch tip strain versus time for a PCBN B, NRR = 150 μm, sample loaded at 1 mm/min. The CZM parameters are, type linear, G_{Ic} = 11 J/m^2, σ_{max} = 1000 MPa. The full transient momentum equation is solved with time step equal to 1 ms. The strain is output by the solver at a cell face corresponding to the exact position of the centre of the TSG in the dynamic experiments described in Section 2.2. A number of observations can be made. Firstly, the striker load prior to fracture is linear with respect to time. The support load is identical to the striker load and is not shown in Figure 21 (a) for clarity. Secondly, the strain close to the notch tip is also linear with respect
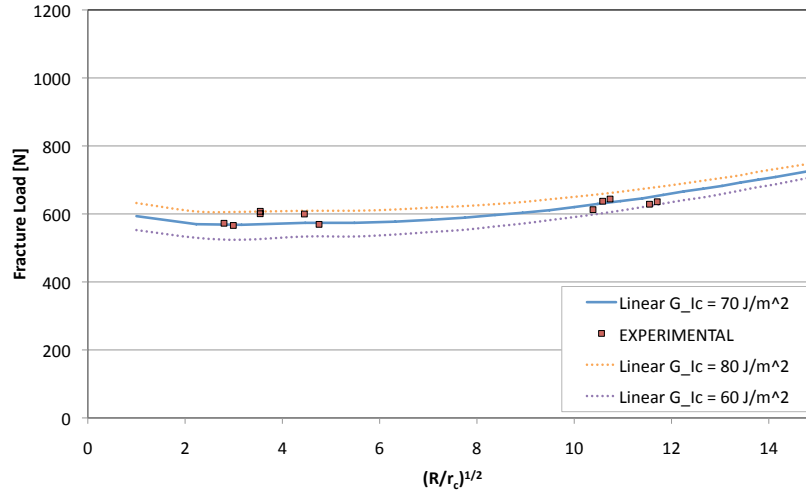
27

Figure 15: The effect of varying G_{Ic} on the fracture load of PCBN A for a variety of normalised notch root radii, R/r_c. σ_{max} was fixed as 600 MPa for all cases and r_c was assumed to be 22 μm. The crosshead displacement rate was 1 mm/min. Results are for linear CZM.

to time. Therefore the load and notch tip strain are linearly proportional to each other.

Figure 21 (b) plots both the numerically predicted striker and support load and the notch tip strain versus time for the same geometry and the same CZM parameters as in Figure 21 (a). The loading rate in this case was 1 m/s and the time step was reduced appropriately to 0.1 μs. A plot of notch tip load is also shown. This is found by multiplying the notch tip strain-time output by the quasi-static proportionality factor, the ratio of quasi-static striker load to quasi-static crack tip strain found in Figure 21 (a). It can be clearly seen that the load at the crack tip is subjected to significantly less dynamic oscillatory effects than either the striker or support load. The striker load is almost zero at the point of fracture. Taking this as the failure load, it
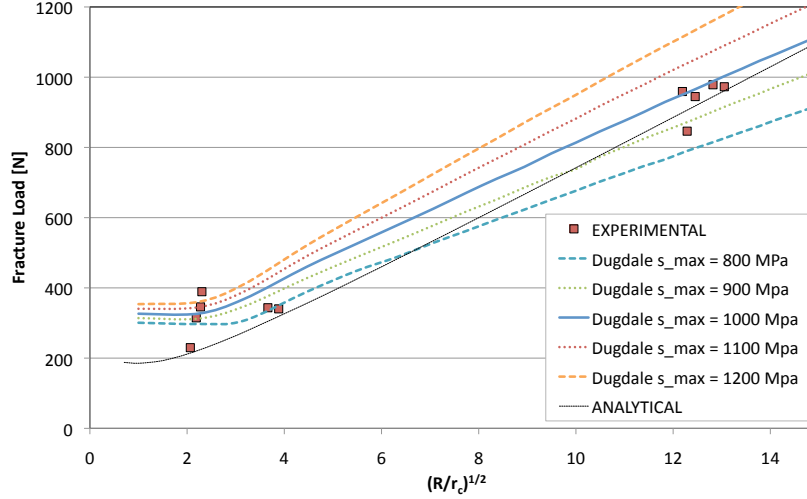
Figure 16: The effect of varying σ_{max} on the fracture load of PCBN B for a variety of normalised notch root radii, R/r_c. G_{Ic} was fixed as 11 J/m^2 for all cases and r_c was assumed to be 1 μm. The crosshead displacement rate was 1 mm/min. Results are for Dugdale CZM.

could be wrongly deduced that the dynamic fracture toughness of PCBN was also almost zero. It should also be noted that the predicted support load for the dynamic case is tensile up until a time of about 3.9 μs. This is because the simulation does not allow for bouncing of the specimen. However, this has a minor influence on the system dynamics once the support load becomes compressive and is not an issue in the current work.

Furthermore, the calibrated failure load as predicted by the notch tip strain gauge is 914 N, the same as the striker failure load for the quasi-static simulation given in Figure 21 (a). Experimental failure loads however at 1 m/s were found to vary widely depending on the stiffness of the striker and supports being used. This indicates that for the range of rates experimentally examined, dynamic effects are not significant and the peak calibrated crack
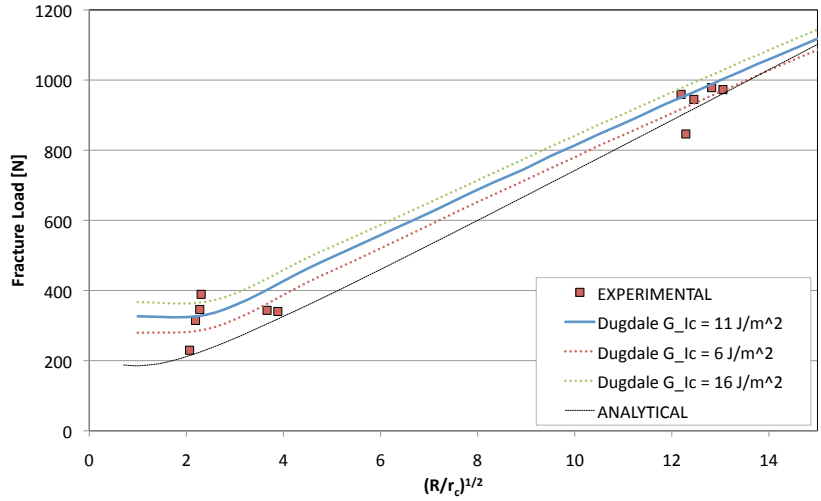
29

Figure 17: The effect of varying G_{Ic} on the fracture load of PCBN B for a variety of normalised notch root radii, R/r_c. σ_{max} was fixed as 1000 MPa for all cases and r_c was assumed to be 1 μm. The crosshead displacement rate was 1 mm/min. Results are for Dugdale CZM.

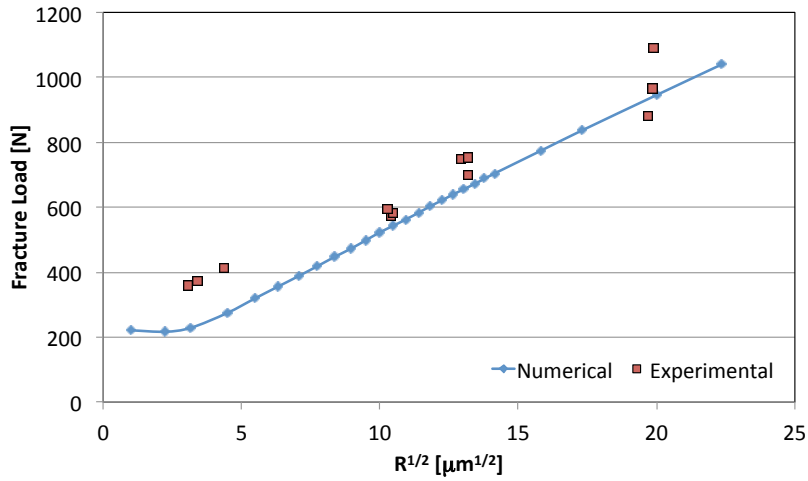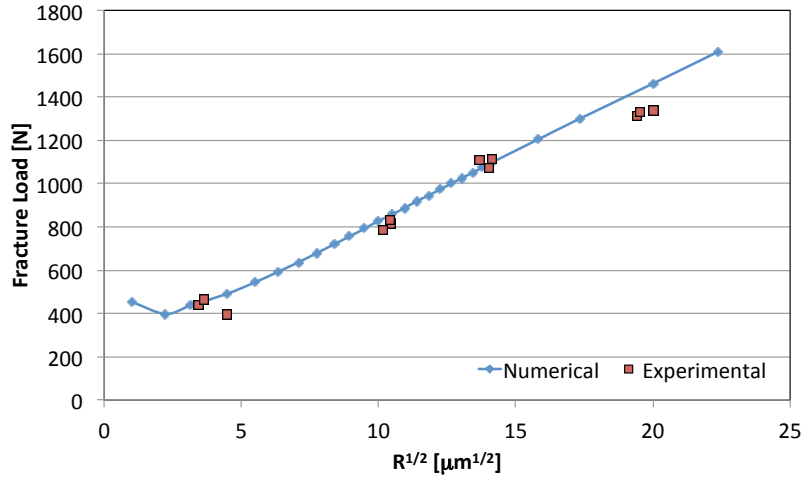Figure 18: Numerical fracture load predictions for PCBN C. $G_{Ic} = 8.7$ J/m^2, $\sigma_{max} = 730$ MPa. A Dugdale CZM is employed.

Figure 19: Numerical fracture load predictions for PCBN D. $G_{Ic} = 38.5$ J/m^2, $\sigma_{max} = 1120$ MPa. A linear CZM is employed.
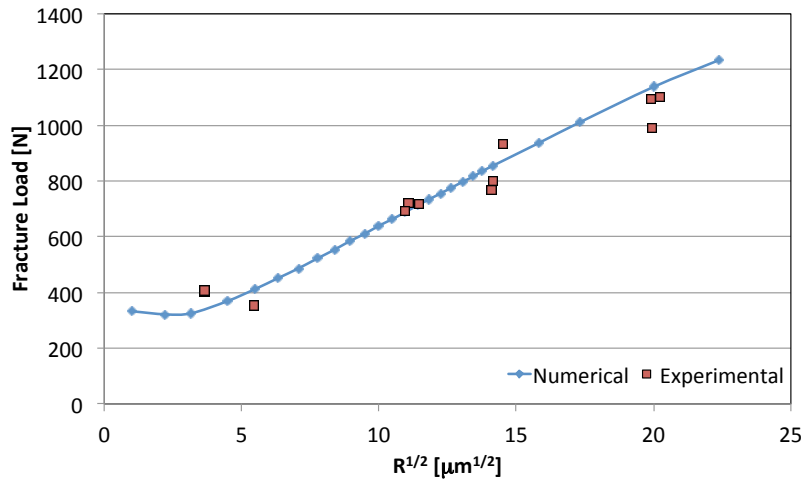

Figure 20: Numerical fracture load predictions for PCBN E. $G_{Ic} = 19.9$ J/m^2, $\sigma_{max} = 875$ MPa. A linear CZM is employed.

31

tip load can be used as an indicator of the failure load. It can also be concluded that the dynamic effects of impact loading are not responsible for the experimentally observed changes in fracture toughness at the rates examined.

This means that the experimentally observed drop in fracture toughness can only be accounted for numerically by changing the parameters of the cohesive zone model. Figure 22 uses the Dugdale model to schematically describe the parameters that can be adjusted. The critical opening displacement, δ_c is set by the selection of G_{Ic} and σ_{max}. $G_{Ic,d}$ represents the dynamic critical fracture energy in Figure 22 while $G_{Ic,s}$ represents the static critical fracture energy.

There are two extremes that may be considered when changing the fracture energy. In the first instance σ_{max} can be kept constant so that $\sigma_{max,d}/\sigma_{max,s} = 1$ and $\delta_{c,d}/\delta_{c,s} = G_{Ic,d}/G_{Ic,s}$. The second extreme is to keep δ_c constant so that $\delta_{c,d}/\delta_{c,s} = 1$ and $\sigma_{max,d}/\sigma_{max,s} = G_{Ic,d}/G_{Ic,s}$. The intermediate option depicted in Figure 22 ensures that the experimentally observed decrease in G follows the locus such that σ_{max}/δ_c is constant. It follows from this that:

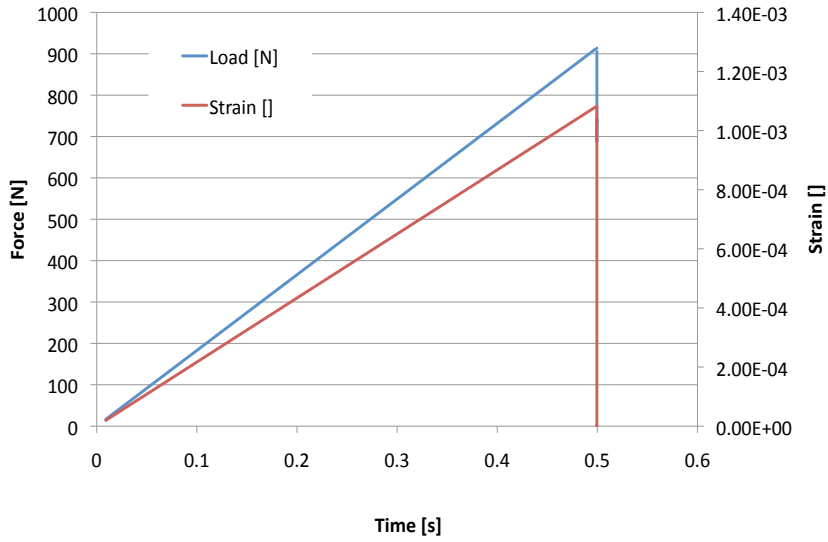$$\sqrt{\frac{G_{Ic,d}}{G_{Ic,s}}} = \frac{\sigma_{max,d}}{\sigma_{max,s}} \tag{8}$$

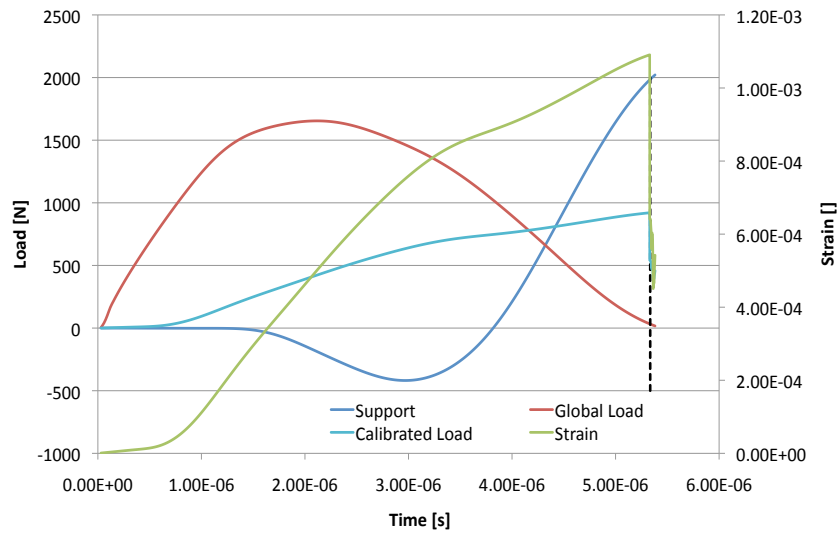And noting that $G_{Ic} \propto K_{Ic}^2$, it follows that:

$$\frac{K_{Ic,d}}{K_{Ic,s}} = \frac{\sigma_{max,d}}{\sigma_{max,s}} \tag{9}$$

Rearranging:

$$\frac{K_{Ic,d}}{\sigma_{max,d}} = \frac{K_{Ic,s}}{\sigma_{max,s}} \tag{10}$$

32

(a) Loading rate $= 1$ mm/min. A straight line relationship between the crack tip strain and the measured striker load is observed.

(b) Loading rate $= 1$ m/s. The failure load as predicted by the tip strain gauge is identical to that predicted for the low rate test.

Figure 21: Effect of rate on the numerically predicted fracture load and for PCBN B, NRR $= 150$ μm, $\sigma_{max} = 1000$ MPa, $G_{Ic} = 11$ J/m^2.
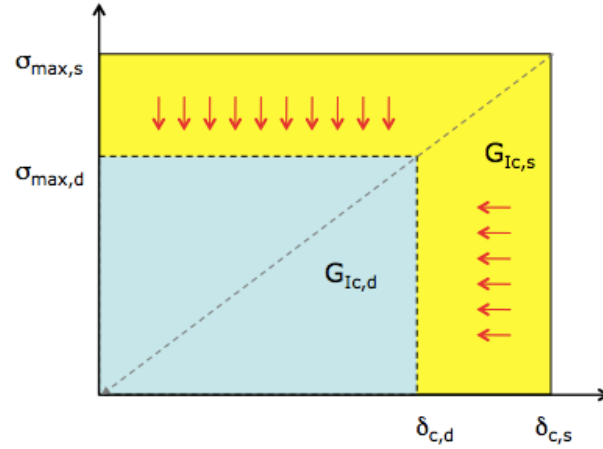
33

Figure 22: The Dugdale model. Parameters can be changed for static and dynamic experimental results. Parameters are G_{Ic}, σ_{max} and δ_c.

Equation (10) indicates that the intermediate option preserves the process zone size/critical distance. Figure 23 plots the average experimentally determined failure loads at rates from 1 mm/min to 1 m/s and the numerically predicted failure loads using the 3 options outlined above. The failure loads are all calculated using the crack tip load from the strain gauge as described above. Excellent agreement is obtained where the constant critical distance is preserved. This is a further indication of the important role that the CBN grain size plays in governing the fracture mechanisms of PCBN material.

8. Conclusions

The fracture toughness of five grade of PCBN was measured across a range of rates and temperatures using a TPB test. It was shown that a unique set of cohesive zone parameters can accurately predict the failure of PCBN for a variety of different notch geometries. The choice of cohesive
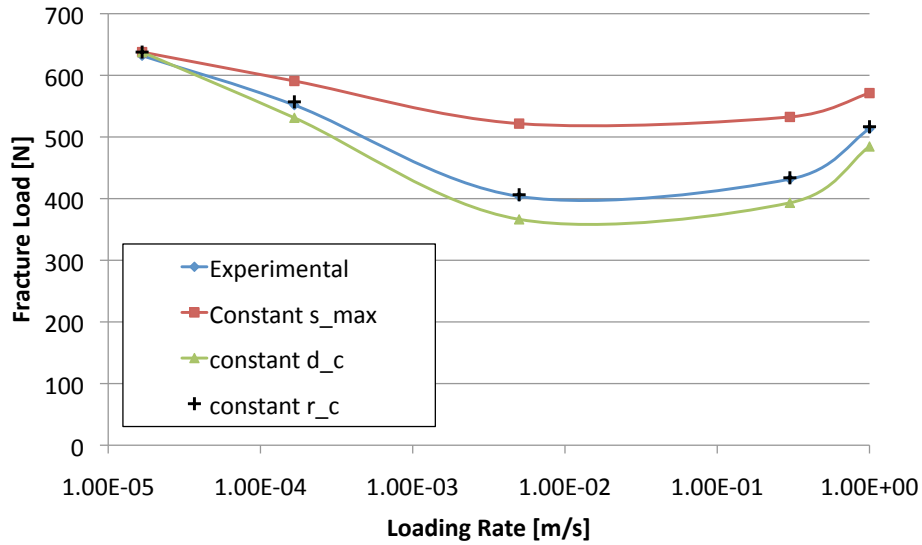
Figure 23: Effect of CZM parameter choice on the numerically predicted fracture load at high rates.

zone shape is also important.

Dynamic effects in the system were found to be insufficient to explain the observed drop in experimentally measured fracture toughness.It was demonstrated that the load at the crack tip is less susceptible to dynamic effects than either the striker or support load. This validates the experimental procedure used in this work for measuring dynamic fracture toughness.

It was demonstrated that in order to accurately predict the experimental failure load as a function of loading rate, the cohesive zone parameters had to be changed in such a way as to preserve the critical distance, r_c, which has been found through the numerous experimental studies in this work to be approximately equal to the grain size.

9. Acknowledgements

References

[1] F. Nabhani, Machining of aerosapce titanium alloys, Robotics and Computer Integrated Manufacturing 17 (2001) 99–106.

[2] I. Petrusha, Cubic boron nitride for cutting nickel base materials, Metal Powder Report 2 (1998) 41.

[3] X. Ding, W. Liew, X. Liu, Evaluation of machining performance of MMC with PCBN and PCD tools, Wear 259 (2005) 1225–1234.

[4] P. Heath, Properties and uses of Amborite, Carbide and Tool Journal 19 (2) (1987) 12–22.

[5] M. Bailey, H. Juchem, M. Cook, J. Collins, P. Butler-Smith, The increasing importance of PCD/diamond/CVDD and PCBN/cBN tooling in the automotive industry, Industrial Diamond Review 62 (592) (2002) 53–60.

[6] M. Fleming, A. Wickham, PCBN in the automotive industry, Industrial Diamond Review 2 (2006) 26–32.

[7] Element Six Ltd. Advanced Materials, PCBN Metalworking, Marketing Brochure.

[8] P. Bex, G. Shafto, The influence of temperature and heating time on PCD performance, Industrial Diamond Review 3 (1984) 128–132.

[9] I. Clark, P. Sen, Advances in the development of ultrahard cutting tool materials, Industrial Diamond Review 2 (1998) 40–44.

[10] M. Cook, P. Bossom, Trends and recent developments in the material manufacture and cutting tool application of polycrystalline diamond and polycrystalline cubic boron nitride, International Journal of Refractory Metals and Hard Materials 18 (2000) 147–152.

[11] D. Taylor, Analysis of fatigue failures in components using the theory of critical distances, Engineering Failure Analysis 12 (2005) 906–914.

[12] D. Taylor, The theory of critical distances, Engineering Fracture Mechanics 75 (2008) 1696–1705.

[13] D. Taylor, Applications of the theory of critical distances in failure analysis, Engineering Failure Analysis 18 (2011) 543–549.

[14] D. Carolan, P. Alveen, A. Ivankovic, N. Murphy, Effect of notch root radius on the fracture toughness of polycrystalline cubic boron nitride, Engineering Fracture Mechanics 78 (17) (2011) 2885–2895.

[15] G. G. F.J. Gomez, M. Elices, Failure criteria for linear elastic materials with u-notches, International Journal of Fracture 141 (2006) 99–13.

[16] BSI, Advanced technical ceramics - Test methods for determination of fracture toughness of monolithic ceramics. Part 5: Single-edge Vee-notch

beam (SEVNB) method, DD CEN 14425-5, British Standards Institution (2004).

[17] D. Rittel, A. Belenky, I. Bar-On, Static and dynamic fracture of transparent nano-grained alumina, Journal of the Mechanics and Physics of Solids 58 (2010) 484–501.

[18] T. Weerasooriya, P. Moy, D. Casem, M. Cheng, W. Chen, A four-point bend technique to determine dynamic fracture toughness of ceramics, Journal of the American Ceramic Society 89(3) (2006) 990–993.

[19] Y. Kim, Y. Chao, Effect of loading rate on dynamic fracture initiation toughness of brittle materials, International Journal of Fracture 145 (2007) 195–204.

[20] J. Kalthoff, On the measurement of dynamic fracture toughness - a review of recent work, International Journal of Fracture 27 (1985) 277–298.

[21] D. Rittel, G. Weisbrod, A method for dynamic fracture toughness determination using short beams, International Journal of Fracture 104 (2000) 89–103.

[22] M. Petrović, Mechanical and fracture properties of polycrystalline diamond as a function of rate and temperature, Ph.D. thesis, University College Dublin (2011).

[23] R. Damani, R. Gstrein, R. Danzer, Critical notch-root radius effect in SENB-S fracture toughness testing, Journal of the European Ceramic Society 16 (7) (1996) 695–702.

[24] R. Ritchie, J. Knott, J. Rice, On the relation between the critical tensile stress and fracture toughness in mild steel, Journal of the Mechanics and Physics of Solids 21 (1973) 395–410.

[25] I. Demirdzić, D. Martinovic, A. Ivanković, Numerical simulation of thermal deformation in welded specimens (in croatian), Zavarivanje 31 (1988) 209–219.

[26] A. Ivanković, I.Demirdzić, J. Williams, P. Leevers, Application of the finite volume method to the analysis of dynamic fracture problems, International Journal of Fracture 66 (1994) 357–371.

[27] A. Karac, A. Ivankovic, Behaviour of fluid filled PE containers under impact: Theoretical and numerical investigation, International Journal of Impact Engineering 36 (2009) 621–631.

[28] A. Ivankovic, Finite volume modelling of dynamic fracture problems, Computer Modelling and Simulation in Engineering 4 (1999) 227–235.

[29] A. Karac, B. Blackman, V. Cooper, A. Kinloch, S. Rodriguez-Sanchez, W. Teo, A. Ivankovic, Modelling the fracture behaviour of adhesively bonded joints as a function of test rate, Engineering Fracture Mechanics 78 (2011) 973–989.

[30] I. Demirdzic, E. Dzaferovic, A. Ivankovic., Finite volume approach to thermoviscoelasticity, Numerical Heat Transfer, Part B 47 (2005) 213–237.

[31] V. Kanyanta, A. Karac, A. Ivankovic, Validation of a fluid structure

interaction numerical model for predicting flow transients in arteries, Journal of Biomechanics 42 (2009) 1705–1712.

[32] A. Ivankovic, K. Pandya, J. Williams, Crack growth predictions in polyethylene using measured traction-separation curves, Engineering Fracture Mechanics 71 (2004) 657–668.

[33] H. Weller, G. Tabor, H. Jasak, C. Fureby, A tensorial approach to CFD using object oriented techniques, Computers in Physics 12 (6) (1998) 620–631.

[34] OpenFOAM Extend Project (-1.6-ext), http://www.extend-project.de.

[35] A. Ivankovic, J. Williams, The finite volume analysis of linear elastic dynamic fracture problems, in: M. Aliabadi (Ed.), Dynamic Fracture Mechanics, Computational Mechanics Publications, Southampton, 1995.

[36] A. Rager, J. Williams, A. Ivankovic, Numerical analysis of the three point bend impact test for polymers, International Journal of Fracture 135 (2005) 199–215.

[37] N. Chandra, H. Li, G. Shet, H. Ghonem, Some issues in the application of cohesive zone models for metal ceramic interfaces, International Journal of Solids and Structures 39 (2002) 2827–2855.

[38] J. Rots, Strain-softening analysis of concrete fracture specimens, in: F. Wittmann (Ed.), Fracture toughness and fracture energy of concrete, Elsevier Science, Amsterdam, 1986, pp. 137–148.

[39] J. Kubler, Fracture toughness of ceramics using the SEVNB method: From a preliminary study to a test method, in: G. Q. J.A. Salem, M. Jenkins (Eds.), Fracture Resistance Testing of Monolithic and Composite Brittle Materials, ASTM International, 2002, pp. 93–106.

[40] M. Elices, G. V. Guinea, J. Gomez, J. Planas, The cohesive zone model: Advantages, limitations and challenges, Engineering Fracture Mechanics 69 (2002) 137–163.

[41] D. Carolan, A. Ivankovic N. Murphy, Thermal shock resistance of polycrystalline cubic boron nitride, Journal of the European Ceramic Society 32 (2012) 2581–2586.